Received: 18 August 2021 | Accepted: 10 November 2021

DOI: 10.1002/maco.202112744

ARTICLE

Materials and Corrosion

Inhibition of corrosion of API K55 steel by tannin from *Acacia mearnsii* bark in highly acidic medium

Katryanne Rohana Georg Bacca | **Natália Feijó Lopes** | **Eleani Maria da Costa**

School of Technology, Pontifical Catholic University of Rio Grande do Sul, Porto Alegre-RS, Brazil

Correspondence
Eleani Maria da Costa, School of Technology, Pontifical Catholic University of Rio Grande do Sul, 6681 Ipiranga Ave, Bldg 30, Room 111/F, 90619-900 Porto Alegre-RS, Brazil.
Email: eleani@pucrs.br

Abstract

The corrosion inhibiting effect of the tannin from *Acacia mearnsii* bark on API 5CT K55 steel, used for casing in the oil and gas industry, was investigated in 1 M HCl medium with different tannin concentrations. Corrosion was monitored by electrochemical tests using potentiodynamic polarization (PP) and electrochemical impedance spectroscopy (EIS). Complementary analyses of the corroded surfaces were performed by scanning electron microscopy (SEM), atomic force microscopy (AFM), and X-ray diffraction (XRD). With the application of *A. mearnsii* tannin, the cathodic branch of the PP curves shifted to lower corrosion current density values. EIS analysis indicated that inhibitor molecules were adsorbed on the steel surface, which provided protection against corrosion. The SEM, AFM, and XRD data showed that in the presence of the inhibitor, a film and amorphous material were adsorbed on the steel surface, plausibly associated with the formation of tannates. The highest inhibition efficiency was obtained at an inhibitor concentration of 0.7 5 g L^{-1} (92% determined by PP and 98% by EIS), and a high degree of surface coverage was observed, compared with that obtained using the other concentrations of tannin.

KEYWORDS

Acacia mearnsii bark, acid medium, corrosion inhibitor, steel, tannin

1 | INTRODUCTION

In the petroleum industry, carbon steels are widely used in components and facilities for the extraction and transportation of oil and gas due to the low cost of this type of steel in relation to that of corrosion-resistant alloys. However, the corrosion resistance of carbon steel is relatively low. From an economic point of view, the impact of corrosion in the oil and gas industry is very high, involving direct and indirect costs associated with lost time, the replacement of materials for construction, and the continuous involvement of personnel in corrosion management, as well as safety and environmental consequences.[1,2] Crude oil and natural gas can carry corrosive substances, such as H_2S, CO_2, and O_2, and water, which act as catalysts for corrosion. Additionally, acidification is widely used to increase oil production. In this technique, a high-temperature acid solution is pumped into the well to create channels in the rocks to allow oil and gas to migrate more easily to the surface and to dissolve rubble found in old wells to restore and maximize productivity.[1–3] The acids used in acidification treatments vary according to the nature of the well and treatment. Some examples of acids used are hydrochloric acid (HCl) 15%–28%, hydrofluoric acid (HF), acetic acid (CHCOOH), chloroacetic acid ($ClCH_3COOH$), formic acid (HCOOH), and sulfamic acid (H_2NSO_3H).[4–6] The acidification technique can exacerbate the corrosion of production tubing, downhole tools, and casing. Thus, it is essential to control the

corrosion to increase the lifetime of the metallic components and facilities, as well as for safety in oil and gas operations. However, corrosion mitigation in the oil and gas industry is a complex process because the fluid characteristics change over time, and the pressure and temperature involved are high. Risks related to corrosion can be minimized by using corrosion inhibitors, applying protective coatings, employing cathodic or anodic protection techniques, and using appropriate corrosion monitoring and inspection techniques.[2,4,7,8] The main factors of concern in selecting a corrosion inhibitor in the oil and gas industry include toxicity, low risk of environmental pollution, availability, and cost. Therefore, developing green corrosion inhibitors for applications in the oil and gas industry is of fundamental importance. Since the 1990s, many studies have been carried out on the use of natural compounds that afford non-toxicity, biodegradability, and can be extracted by simple procedures at a relatively low cost.[9–16] Tannins are recognized as natural corrosion inhibitors, as they have antioxidant properties derived from the polyphenolic and flavonoid groups in their structure. Tannins are present in many herbs, trees, fruits, and legumes, providing vast variability in structure and molecular weight.[17] Metal protection is provided by the adsorption of compounds in the extract of plants on the metal surface.[11,12,14,18]

Acacia mearnsii (de Wild) is a very common hardwood species cultivated in several countries, and its bark contains large amounts of tannins. The recoverable tannins can reach up to 30% of the dry weight depending on the extraction process employed.[17] The tannin from *A. mearnsii* bark is a condensed tannin that is already industrially produced on a large scale. In aqueous solutions, tannins react with metallic ions to form a protective monolayer composed of tannates on the metal surface, acting as a barrier for the corrosion process. Tannates are amorphous in nature and are usually insoluble in aqueous solutions.[11,12,14–16,18–20] Few studies have evaluated the inhibition of metal corrosion by *A. mearnsii* tannin. Guedes et al.[12] and Rodrigues et al.[18] employed tannin from *A. mearnsii* bark as a corrosion inhibitor for aluminum alloys, and Gerengi et al.[11] demonstrated that this inhibitor offers good performance in controlling corrosion. Peres et al.[14] and Rahim et al.[15,16] also achieved high inhibitory efficiencies for carbon steel. Peres et al.[14] tested plain carbon steel (1% C) in aerated 0.1 mol L^{-1} Na_2SO_4 (pH 6.0 and 2.5) using a fixed tannin concentration of 2 g L^{-1}, where the best anticorrosion activity was found at pH 2.5. These previous studies have shown that the anticorrosion activity of tannin from *A. mearnsii* bark is very satisfactory in acidic environments and that its efficiency depends on the tannin concentration.[11,12,14,18] Martinez and Stern[20] studied the mechanism of adsorption of tannins on low-carbon steel in the presence of sulfuric acid at pH 1, 2, and 3 using a concentration range of 10^{-5} to 10^{-1} mol L^{-1} of tannin. At pH 1 and 2, the value of the adsorption free energy suggests a chemisorption mechanism due to bonding between the oxygen lone-pair electrons of the tannin −OH group and the metal surface, while at pH ≥ 3, ferric tannate is formed, and the free energy of adsorption suggests a physisorption mechanism. However, there is no consensus on the appropriate tannin concentrations to be used because the adsorption efficiency is highly dependent on the metal, temperature, pH, and medium, and the anticorrosion mechanisms are not fully understood. The present work aims to investigate the mechanisms by which tannin from *A. mearnsii* bark inhibit the corrosion of API K55 steel used for casing in oil fields in 1 M HCl medium.

2 | MATERIALS AND METHODS

2.1 | Preparation of steel specimen

API K55 carbon steel from a typical oil well casing[21] was used as the test specimen. Table 1 shows the chemical composition obtained by optical emission spectroscopy (SPECTROMAXx from AMETEK Materials Analysis Division®). The steel microstructure is shown in Figure 1 and is composed of ferrite and perlite.

Before the corrosion tests, the samples were embedded in acrylic resin, mechanically polished with silicon carbide paper of different grades (≠220 up to ≠1200), rinsed with distilled water, cleaned with acetone, and dried with hot air. The electrical contact was made with a copper wire using a silver bonder.

TABLE 1 Chemical composition of API K55 steel (wt.%)

C	Si	Mn	P	S	Cr	Ni	Mo	Fe
0.235	0.239	1.35	0.022	0.0089	0.036	0.015	0.016	Remaining
Al	**Cu**	**Ti**	**Co**	**Nb**	**Sn**	**Bi**	**Zr**	
0.022	0.0096	0.0020	<0.0015	<0.0030	0.011	<0.0020	0.0018	

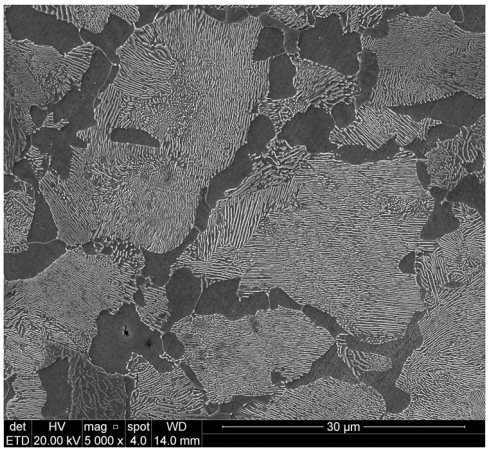

FIGURE 1 Microstructure of API K55 steel

2.2 | Preparation of inhibitor solution

A. mearnsii tannin (Weibull AQ) was used as an inhibitor. This tannin was extracted from the bark of *A. mearnsii* de Wild with hot water, and then spray-dried to produce the extract in the form of a powder. According to the manufacturer, *A. mearnsii* tannin is rich in colloidal tannins, with a high number of nontoxic phenolic dihydric nuclei, containing at least 93.5% active matter, and the pH is 4.5–5.5 (20 vol.% in aqueous solution). Chemically, acacia tannin is a mixture of complex substances, such as condensed polyphenols, mainly flavan-3-4-diol, in addition to other substances such as sugars and hydrolysable gums. The tannin powder was weighed using a 0.0001 g precision balance and then diluted to different concentrations (0, 0.25, 0.50, 0.75, 1.0, and 1.5 g L^{-1}) in 1 M HCl aqueous solution (pH = 0.42). After preparation, the solution was homogenized for 30 min using a magnetic stirrer. The concentrations above were limited to 1.5 g L^{-1} to avoid non-dissolved tannin particles in solution, as Peres et al.[14] observed that at concentrations above 2 g L^{-1}, particles were visible in Na_2SO_4 solutions at room temperature.

2.3 | Electrochemical measurements

Potentiodynamic linear polarization (PP) and electrochemical impedance spectroscopy (EIS) were used to study the corrosion behavior of API K55 steel exposed to different concentrations of tannin in 1 M HCl solution at room temperature. The electrochemical measurements were performed using a three-electrode cell connected to an Autolab potentiostat/galvanostat (PGSTAT302 N model). The electrochemical cell was composed of a platinum wire counter electrode (CE), a saturated calomel reference electrode (SCE), and an API K55 steel sample as the working electrode (WE), with an exposed area of approximately 1 cm^2. All electrochemical measurements were performed in triplicate under aerated conditions, and all potentials are referenced to the SCE ($E = 241$ mV vs. NHE).

Before each electrochemical measurement, the working electrode was immersed in the test solution for 1 h to attain a steady-state open circuit potential (OCP). The EIS analysis was conducted at a frequency of 10,000 to 0.1 Hz and an amplitude of ±10 mV. The electrical parameters were obtained from the EIS data by fitting, using ZView software. The PP measurements were performed in the voltage range of −300 to +300 mV in relation to the value for the OCP obtained at a scan rate of 1 mV s^{-1}. Autolab Nova 1.1 software was used to analyze the electrochemical data from the PP curves by the Tafel extrapolation method.

Equation (1) was used to calculate the inhibition efficiency E (%), as obtained by potentiodynamic polarization and EIS techniques:

$$E(\%) = \frac{(Rp_o - Rp_i)}{Rp_i} \times 100, \quad (1)$$

where Rp_o and Rp_i are the polarization resistances of API K55 steel in 1 M HCl with and without the inhibitor, respectively.

After approximately 3 h, each test was completed, and the samples were washed with distilled water, dried with hot air, and placed in a desiccator for further characterization of the corroded surface.

2.4 | Characterization of corroded surface

Scanning electron microscopy (SEM), X-ray diffraction (XRD), and atomic force microscopy (AFM) were used to characterize the corroded surfaces. For SEM analysis, a field-emission scanning electron microscope (F50-FEI) was used; the samples were pretreated by coverage with gold. A Shimadzu diffractometer with a copper source was used for the XRD analyses using conditions of 40 kV and 30 mA; the angle was varied from θ–$2\theta = 10°$–$80°$ with a step size of 0.05°, over a time of 0.3 s. AFM analysis was performed using a Bruker Dimension Icon PT microscope, with a scanning area of 8100 μm^2.

3 | RESULTS AND DISCUSSION

Figure 2 shows the OCP during 1 h of measurement, and Figure 3 shows the potentiodynamic polarization curves for the different concentrations of inhibitors

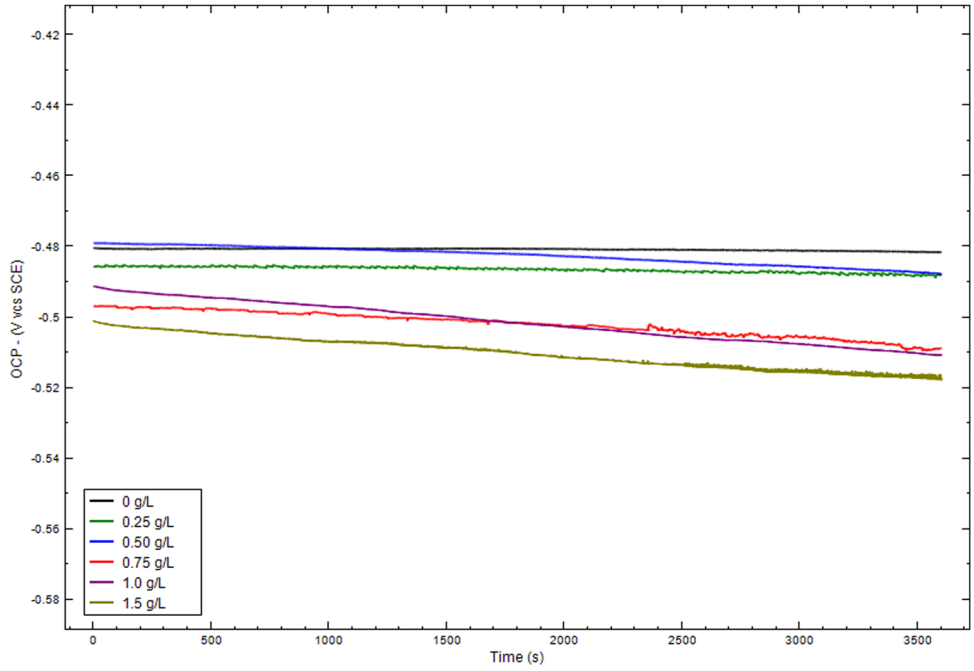

FIGURE 2 Open circuit potential (OCP) for API K55 steel in 1 M HCl medium with different concentrations of *Acacia mearnsii* tannin [Color figure can be viewed at wileyonlinelibrary.com]

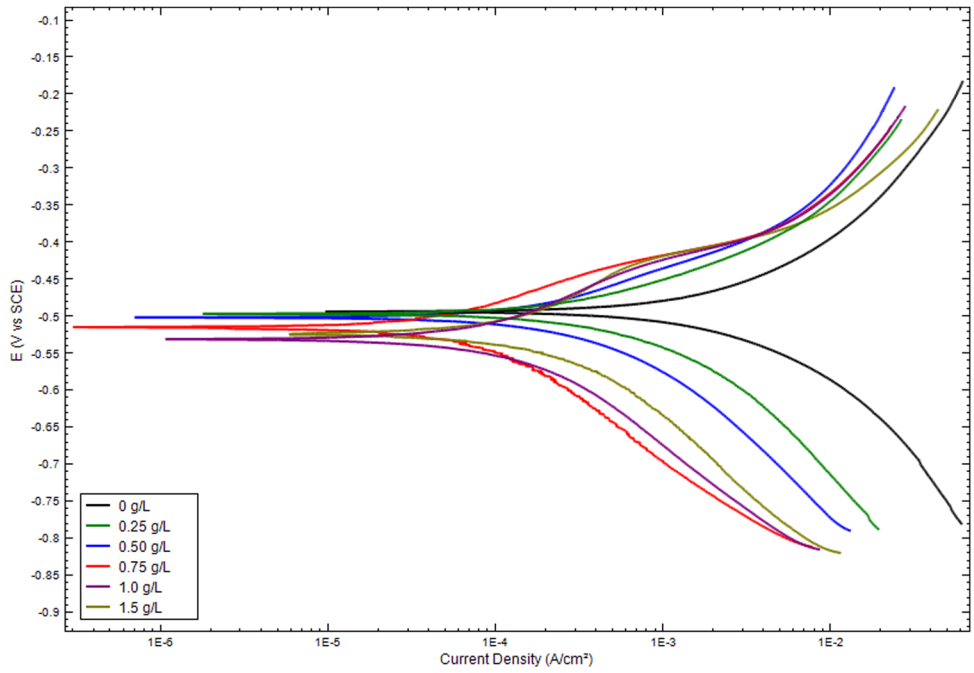

FIGURE 3 Polarization curves for API K55 steel in 1 M HCl medium with different concentrations of *Acacia mearnsii* tannin [Color figure can be viewed at wileyonlinelibrary.com]

used in 1 M HCl medium. Table 2 shows the electrochemical parameters (corrosion potential [E_{corr}], corrosion current density [j_{corr}], and polarization resistance [R_p]) obtained from the potentiodynamic polarization curves by the Tafel extrapolation method, and the inhibition efficiencies were calculated by applying Equation (1).

The potentials (Figure 2) remained relatively stable during 1 h of the OCP measurements for tannin concentrations of 0 and 0.25 g L^{-1}, whereas for 0.50, 0.75,

TABLE 2 Electrochemical parameters obtained by PP and inhibition efficiency for API K55 steel in 1 M HCl medium with different concentrations of *Acacia mearnsii* tannin

Tannin concentration (gL^{-1})	E_{corr} (mV)	j_{corr} ($mAcm^{-2}$)	R_p (Ωcm^2)	Inhibitor efficiency (%)
0	−493	3.57	10	–
0.25	−496	1.40	31	67
0.50	−501	1.08	42	75
0.75	−558	0.22	160	92
1.0	−530	0.32	80	87
1.5	−523	0.39	66	84

Abbreviation: PP, potentiodynamic polarization.

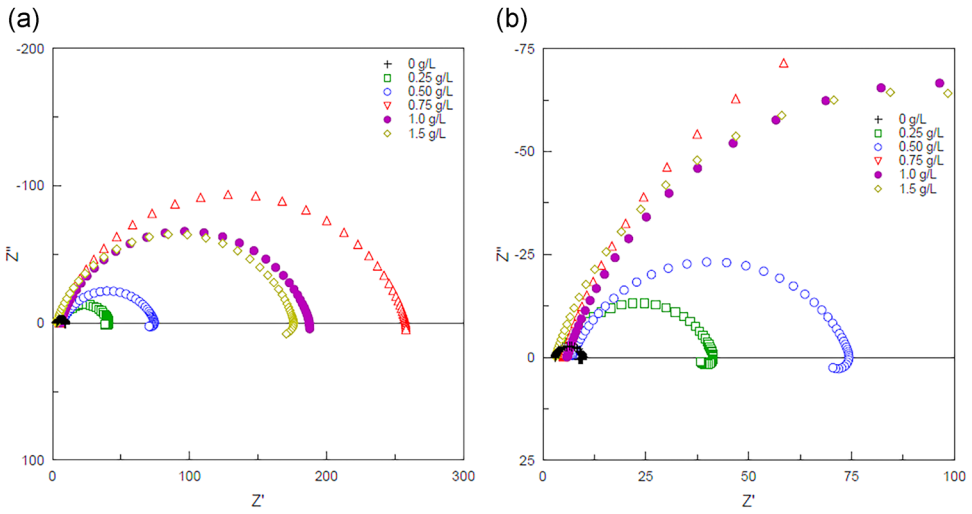

FIGURE 4 (a) Nyquist diagrams for API K55 steel in 1 M HCl medium with different concentrations of *Acacia mearnsii* tannin. (b) Amplification of the first phase of (a) [Color figure can be viewed at wileyonlinelibrary.com]

1.0, and 1.5 g L^{-1} of inhibitor, the potentials decreased slightly over time in the direction of more active potentials. The polarization curves (Figure 3) show that the corrosion potentials changed by no more than 65 mV in the direction of more active values as the inhibitor concentration increased, and the anodic and cathodic branches shifted to lower current densities in the presence of the inhibitor. This indicates that *A. mearnsii* tannin acts as a mixed inhibitor. However, the cathodic branch of the polarization curves was more strongly influenced by the inhibitor, indicating that this tannin is more effective in reducing the hydrogen reaction for API steel K55 in 1 M HCl medium, as found by Guedes et al.[12] for AA 7075 aluminum alloy. The highest inhibition efficiency was obtained when the concentration of *A. mearnsii* tannin was 0.75 g L^{-1}, reaching an inhibitor efficiency of 92%, possibly due to the formation of a more homogeneous layer of tannate compounds on the steel surface. The inhibition efficiency decreased slightly for inhibitor concentrations of 1.0 and 1.5 g L^{-1}, which may be related to the formation of a porous layer or weak adsorption of the inhibitor and consequent desorption, as also observed by Bacca et al.[9]

EIS data were obtained after 1 h of immersion of the steel in the medium to obtain information about the surface properties with and without the addition of the inhibitor to better understand the mechanism of inhibition. Figure 4 presents the Nyquist plots for the different inhibitor concentrations, which show a single capacitive arc and a small inductive loop for each system. Furthermore, the shape of the arcs did not change with the addition of the inhibitor, indicating that the mechanism of steel dissolution was not modified in the presence of the inhibitor, as also observed in the PP curves in Figure 2. However, the diameter of the steel capacitive arc changed according to the concentration of the inhibitor; the larger the diameter of the arc, the greater the resistance to polarization and, consequently, the lower the corrosion rate. The diameter of the capacitive arcs increased with inhibitor concentrations of up to

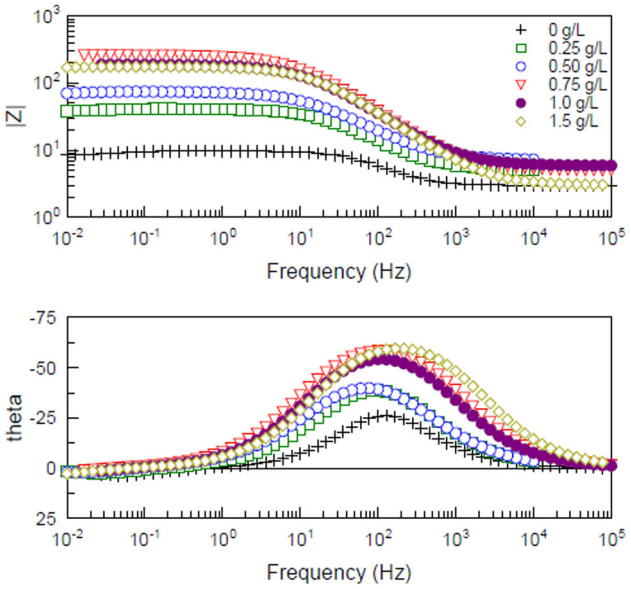

FIGURE 5 Bode diagrams for API K55 steel in 1 M HCl medium for different concentrations of *Acacia mearnsii* tannin [Color figure can be viewed at wileyonlinelibrary.com]

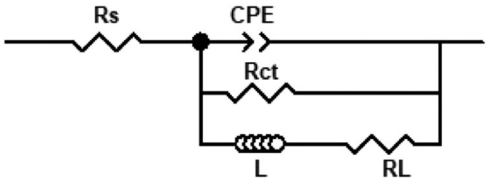

FIGURE 6 Equivalent circuit. *CPE*, constant phase; R_{ct}, charge transfer resistance; RL and L, resistive and inductive elements; R_s, resistance of the solution

0.75 g L^{-1}, whereas for inhibitor concentrations of 1 and 1.5 g L^{-1}, the diameter of the capacitive arc decreased slightly, in accordance with the PP results. This behavior indicates that corrosion is mainly a charge transfer-controlled process. The inhibitor molecules adsorbed on the metallic surface dislocate water molecules and adsorbed ions from the surface, decreasing their electrical capacity. The small inductive loop observed at low frequencies may be associated with the relaxation of the adsorption of intermediate species due to corrosion or adsorption of the inhibitor molecules on the metal surface. The relaxation phenomenon has been reported in the literature and is frequently associated with distinct adsorbed species, such as H^+, Cl^-, O^{2-}, or inhibitor species on the metal surface.[10]

The Bode diagrams (Figure 5) show that both the impedance modulus |Z| and the theta phase angle increased as the inhibitor concentration increased up to 0.75 g L^{-1} because the inhibitor is more strongly adsorbed on the steel surface. The plots show only one time constant, with a maximum phase angle of approximately −65° for an inhibitor concentration of 0.75 g L^{-1}, associated with the high capacitive character of the film formed.

Tests were performed based on the EIS data to approximate the results to an electrical equivalent circuit. The most suitable circuit (best fitting) is shown in Figure 6, where R_s represents the resistance of the solution, R_{ct} is the charge transfer resistance, and *CPE* is the constant phase element, which represents a nonideal capacitor, generally associated with a surface that is not homogeneous. The *CPE* value depends on the roughness and heterogeneity of the surface; RL and L represent the resistive and inductive elements of the circuit.

An electrical double layer is formed when two conductive phases (solid/liquid) are brought into contact, generating an electrochemical interface known as a double layer, characterized by an electrical charge distribution. Equation (2) was used to calculate the double-layer capacitance (C_{dl}) values:

$$C_{dl} = CPE\,(\omega_{max})^{(n-1)}, \tag{2}$$

where *CPE* represents the constant phase element, ω_{max} represents the highest peak intensity from the Nyquist diagram, and n represents the degree of surface homogeneity.

Table 3 presents the electrical parameters obtained from the EIS data. The values of R_{ct} and C_{dl} were higher in the presence of the corrosion inhibitor, where the highest value was found for the inhibitor concentration of 0.75 g L^{-1}. This is probably due to the decrease in the local dielectric constant and/or the increased thickness of the electrical double layer due to the inhibitor molecules adsorbed on the metal surface. The highest inhibition efficiency was achieved for the inhibitor concentration of 0.75 g L^{-1}, consistent with the PP data. The inhibition efficiency for this concentration obtained by EIS was 98%, while that obtained using PP was 92%. The EIS data show no significant difference in the inhibition efficiency for the inhibitor concentrations of 0.75, 1.0, and 1.5 g L^{-1}; however, at 0.75 g L^{-1}, a more protective film was formed.

After the electrochemical tests, complementary analysis of the steel corroded surface was performed using field-emission SEM, XRD, and AFM. Observation of the steel surface after the corrosion tests in tannin solutions revealed the formation of a film on the steel surface. However, this film was not blue-black, as observed when ferric-tannate compounds are formed at higher pH.[14,15,20] Figure 7 shows the SEM images of the API K55 steel surface for different *A. mearnsii* tannin concentrations. The SEM images of the steel surfaces exposed to the corrosive solution without the inhibitor (Figure 7a) show irregularities, due to the preferential dissolution of ferrite.

TABLE 3 Electrochemical parameters from EIS for different inhibitor concentrations

Tannin concentration (g L^{-1})	R_s (Ω)	R_{ct} (Ω cm^{-2})	n	L (H cm^{-2})	R_L (Ω cm^{-2})	C_{PE} (F cm^{-2})	C_{dl} (F cm^{-2})	R_p (Ω cm^{-2})	Inhibitor efficiency (%)
0	3	7	0.86	113	32	8.38×10^{-4}	4.81×10^{-4}	5	–
0.25	5	37	0.80	1941	330	4.98×10^{-4}	2.66×10^{-4}	33	83
0.50	7	68	0.77	7727	670	4.33×10^{-4}	2.26×10^{-4}	61	91
0.75	3	285	0.84	35 404	2613	8.28×10^{-5}	5.47×10^{-5}	256	98
1.0	6	183	0.80	42 346	1941	1.62×10^{-4}	9.79×10^{-5}	166	97
1.5	3	174	0.81	37 923	1514	1.41×10^{-4}	8.78×10^{-4}	155	96

Abbreviation: EIS, electrochemical impedance spectroscopy.

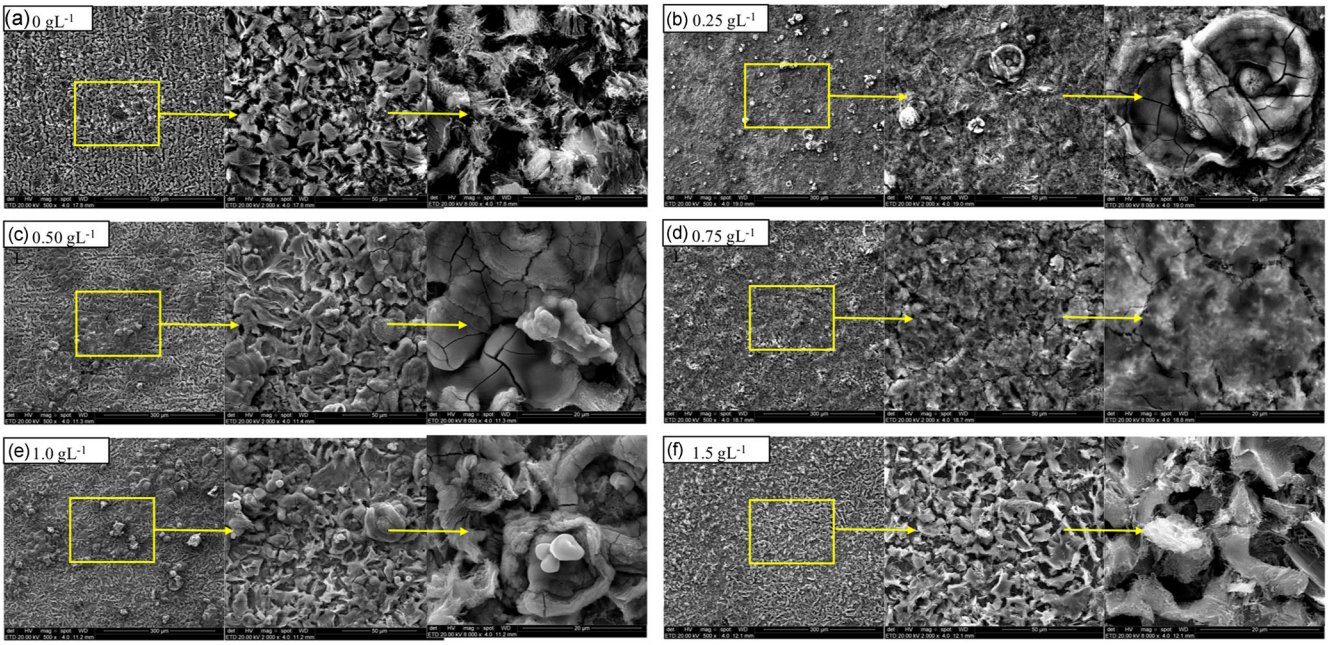

FIGURE 7 SEM images of API K55 steel surface corroded in 1 M HCl with different inhibitor concentrations. (a) 0 gL^{-1}, (b) 0.25 gL^{-1}, (c) 0.5 gL^{-1}, (d) 0.75 gL^{-1}, (e) 1.0 gL^{-1} and (f) 1.5 0 gL^{-1} of *Acacia mearnsii* tannin. SEM, scanning electron microscopy [Color figure can be viewed at wileyonlinelibrary.com]

In the presence of the inhibitor (Figures 7b–e), a black film with a morphology similar to that of iron-tannate was formed on the steel surface.[15] For tannin concentrations of 0.25, 0.50, 1.0, and 1.5 g L^{-1}, the films were less homogeneous than for those formed with 0.75 g L^{-1}, with a lower degree of surface coverage for the former. The SEM image in Figure 8a shows an area where the corroded steel surface is coated with the film, along with an uncoated region. The energy-dispersive X-ray spectroscopy (EDX) spectrum of the uncoated region (Figure 8b) show the typical elements present in the steel chemical composition (Fe, C, and Mn), whereas, in the coated area (Figure 8c), the elements detected by EDX are Fe, C, and O, indicating the formation of iron-tannate.

AFM images of the corroded surface are shown in Figure 9. The surface roughness values, namely, the quadratic roughness (R_q), mean roughness (R_a), and maximum roughness (R_{max}), are summarized in Table 4. The AFM images and surface roughness data for the corroded surface show that the roughness was higher for the corroded steel in the presence of the inhibitor. This may be an indication that inhibitor molecules were adsorbed on the steel surface during the corrosive process, corroborating the results obtained by electrochemical techniques and SEM. For the concentrations of 0.25 and 0.50 g L^{-1} of tannin, the roughness was similar but was higher than in the case of the steel corroded without the addition of the inhibitor and in the presence of the

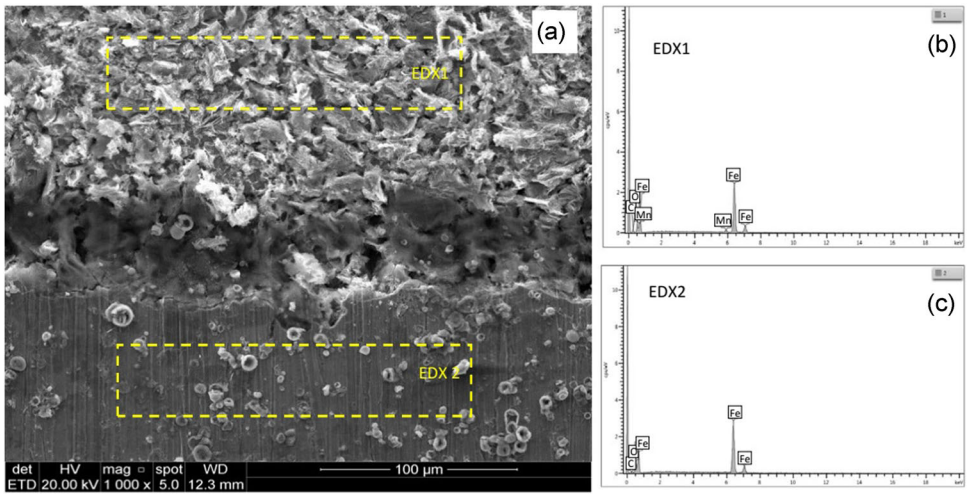

FIGURE 8 (a) SEM image of API K55 steel surface after corrosion in presence of tannin as inhibitor showing two regions, coated and uncoated. (b) EDX spectrum of uncoated region. (c) EDX spectrum of coated region. EDX, Energy-dispersive X-ray spectroscopy; SEM, scanning electron microscopy [Color figure can be viewed at wileyonlinelibrary.com]

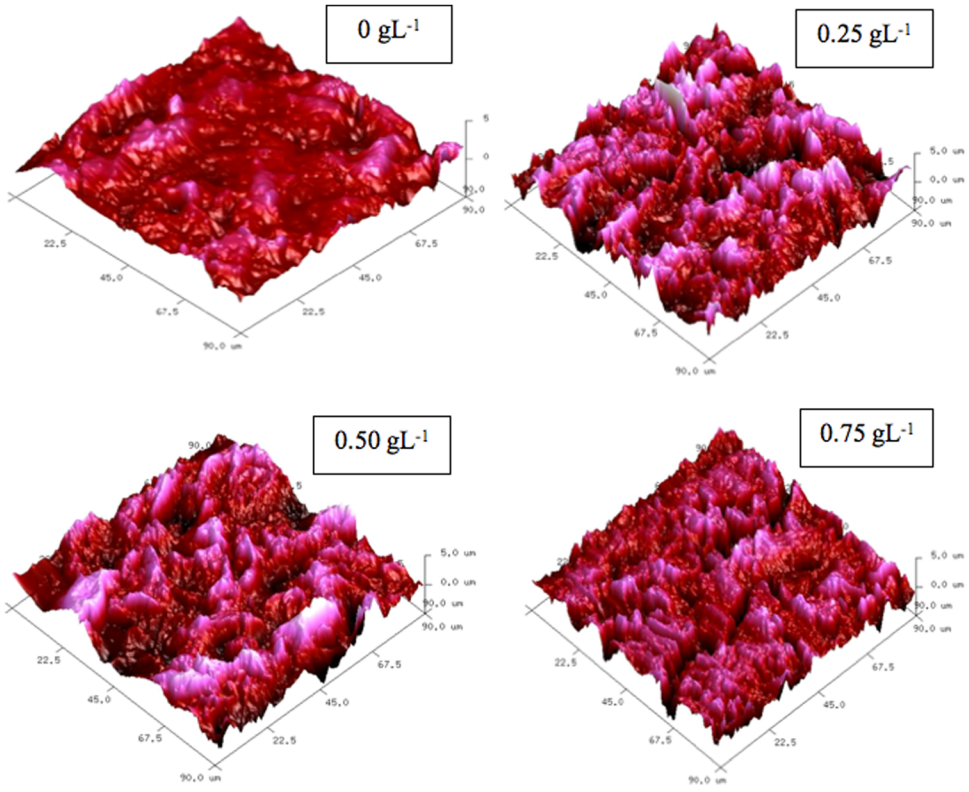

FIGURE 9 3D AFM images of API K55 steel surface corroded in 1 M HCl medium with and without the addition of corrosion inhibitor. 3D, three dimensional; AFM, atomic force microscopy [Color figure can be viewed at wileyonlinelibrary.com]

inhibitor at a concentration of 0.75 g L^{-1}, plausibly due to the presence of an adherent inhibitor film that is not uniform and/or does not fully cover the steel surface. With an inhibitor concentration of 0.75 g L^{-1}, the roughness was lower than that obtained with concentrations of 0.25 and 0.50 g L^{-1}, which may be related to the formation of a more homogeneous and uniform protective layer rather than full coverage of the metal surface, confirming that the highest inhibition efficiency was achieved with an inhibitor concentration of 0.75 g L^{-1}.

TABLE 4 Roughness values obtained from AFM for API K55 steel surface corroded in 1 M HCl medium with and without the addition of corrosion inhibitor

Tannin concentration (g L^{-1})	R_q (nm)	R_a (nm)	R_{max} (nm)
0	628	483	8362
0.25	1399	1120	10 209
0.50	1393	1110	12 556
0.75	1153	888	8969

Abbreviation: AFM, atomic force microscopy.

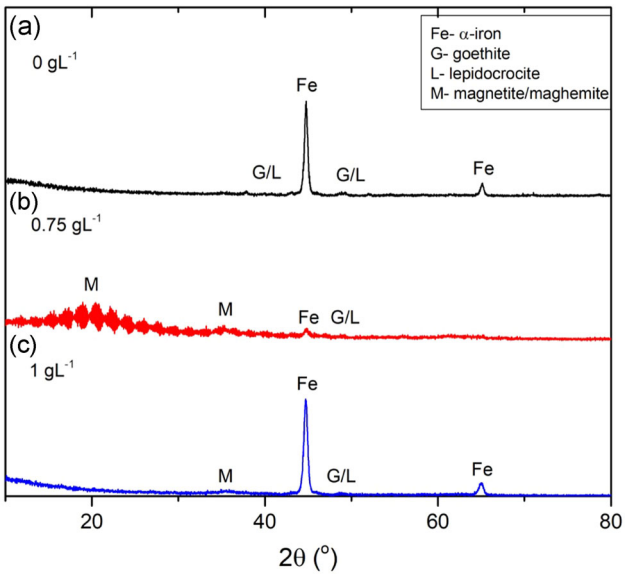

FIGURE 10 Diffractograms of the corrosion products formed on the surface of the samples with and without inhibitor [Color figure can be viewed at wileyonlinelibrary.com]

XRD was used to determine the formation of crystalline corrosion products. The analysis was performed using a bulk sample. The X-ray spectrum of the sample corroded in the medium without the addition of the inhibitor (Figure 10a) shows only characteristic iron peaks (α-Fe) at angles of 45° and 65° and very low-intensity peaks of iron hydroxides (goethite and lepidocrocite). The profile of the sample corroded with 0.75 g L^{-1} of inhibitor (Figure 10b) presented additional enlarged peaks at approximately 20° and 35°, indicating the presence of iron oxides (Fe_3O_4-magnetite or Fe_2O_3-maghemite). The enlarged peaks are plausibly related to amorphous products. Of note, iron-tannates are amorphous.[15,16,19] The α-Fe peak at 45° was also present in the X-ray spectrum, but of lower intensity, indicating that the surface was not completely covered by the film. With the addition of 1.0 g L^{-1} of inhibitor (Figure 10c), the characteristic Fe peaks were observed at 45° and 65°, in addition to the presence of a small amount of amorphous products, indicating that part of the surface is not fully covered with protective film, corroborating the electrochemical results and SEM images.

4 | CONCLUSION

From the analysis of the corrosion inhibition of API K55 steel by tannin of *A. mearnsii* bark in 1 M HCl medium, the following conclusions can be drawn:

- The potentiodynamic polarization curves showed that the tannins from *A. mearnsii* bark mainly influence the cathodic reactions, shifting the corrosion current density to lower values.
- Electrochemical analyses show that *A. mearnsii* bark tannin provides high inhibition efficiency at a concentration of 0.75 g L^{-1} (92% as determined by PP and 98% from EIS).
- The Nyquist and Bode diagrams confirm the results obtained in the potentiodynamic polarization tests, indicating the adsorption of a film of inhibitor molecules on the steel surface, which provides protection against corrosion. SEM and AFM images of the steel surfaces exposed to different inhibitor concentrations and the surface roughness data confirm the formation of an adsorbed film on the steel surface in the presence of the inhibitor. The degree of surface coating and the properties of the protective film depend on the concentration of the inhibitor used.
- XRD analyses indicate that in the presence of the inhibitor, an amorphous material is deposited on the steel surface, possibly associated with the formation of tannates.
- All results showed that the tannin of *A. mearnsii* bark presents high performance as a corrosion inhibitor for API steel in acid medium, and is promising in many industrial sectors, including the oil industry. The fact that it is already commercially available is an important advantage.

ACKNOWLEDGMENTS

The authors acknowledge the support provided by CNPq (The Brazilian Research Council) and TANAC A.S for providing tannins. This study was financed in part by the Coordenação de Aperfeiçoamento de Pessoal de Nivel Superior—Brasil (CAPES)—Finance Code 001.

CONFLICT OF INTERESTS

The authors declare that there are no conflict of interests.

DATA AVAILABILITY STATEMENT

Research data are not shared.

ORCID

Eleani Maria da Costa http://orcid.org/0000-0001-8733-3083

REFERENCES

[1] L. Popoola, A. Grema, G. Latinwo, B. Gutti, A. Balogun, *Int. J. Ind. Chem.* **2013**, *4*, 506.
[2] P. Rajeev, A. O. Surendranathan, C. S. N. Murthy, *J. Mater. Environ. Sci.* **2012**, *3*, 856.
[3] K. Haruna, I. B. Obot, N. K. Ankah, A. A. Sorour, T. A. Saleh, *J. Mol. Liq.* **2018**, *264*, 515.
[4] A. Singh, M. A. Quraishi, *J. Mater. Environ. Sci.* **2015**, *6*, 224.
[5] D. Jayaperumal, *Mater. Chem. Phys.* **2010**, *119*, 478.
[6] S. Vishwanatham, N. Haldar, *Corros. Sci.* **2008**, *50*, 2999.
[7] M. Askari, M. Aliofkhazraei, R. Jafari, P. Hamghalam, A. Hajizade, *Appl. Surf. Sci. Adv.* **2021**, *6*, 100128.
[8] A. A. Olajire, *J. Mol. Liq.* **2017**, *248*, 775.
[9] K. Bacca, N. F. Lopes, J. B. Marcolino, F. Grasel, E. M. Costa, *Mater. Corros.* **2020**, *71*, 155.
[10] N. Chaubey, V. K. Singh, M. A. Quraishi, *Ain Shams Eng. J.* **2018**, *9*, 1131.
[11] H. Gerengi, K. Schaefer, H. I. Sahin, *J. Ind. Eng. Chem.* **2012**, *18*, 2204.
[12] L. A. L. Guedes, K. G. Bacca, N. F. Lopes, E. M. Costa, *Mater. Corros.* **2019**, *70*, 1288.
[13] D. Kesavan, M. Gopiraman, N. Sulochana, *Chem. Sci. Rev. Lett.* **2012**, *1*, 1.
[14] R. S. Peres, E. Cassel, D. S. Azambuja, *ISRN Corros.* **2012**, *1*, Article ID 937920.
[15] A. A. Rahim, E. Rocca, J. Steinmetz, M. J. Kassim, R. Adnan, M. S. Sani Ibrahim, *Corros. Sci.* **2007**, *49*, 402.
[16] A. A. Rahim, J. Kassim, *Recent Pat. Mater. Sci.* **2008**, *1*, 223.
[17] S. Ogawa, Y. Yazaki, *Molecules* **2018**, *23*, 837.
[18] S. R. S. Rodrigues, V. Dalmoro, J. H. Z. Santos, *Mater. Corros.* **2020**, *71*, 1160.
[19] O. Lahodny-Šarc, F. Kapor, *Mater. Corros.* **2002**, *53*, 264.
[20] S. Martinez, I. Štern, *J. Appl. Electrochem.* **2001**, *31*, 973.
[21] API Specification 5CT, *Specification for Casing and Tubing*, American Petroleum Institute, Washington, DC **2006**.

How to cite this article: K. R. G. Bacca, N. F. Lopes, E. M. da Costa. Inhibition of corrosion of API K55 steel by tannin from *Acacia mearnsii* bark in highly acidic medium. *Mater. Corros.* **2022**;73:613–622.
https://doi.org/10.1002/maco.202112744